Research Square

Preprints are preliminary reports that have not undergone peer review.
They should not be considered conclusive, used to inform clinical practice,
or referenced by the media as validated information.

Internet gaming disorder: dynamic functional connectivity and graph theory

Yichen Guo
The First Affiliated Hospital of Zhengzhou University
Guohao Lu
The First Affiliated Hospital of Zhengzhou University
Xinyu Wang
The First Affiliated Hospital of Zhengzhou University
Wenjing Li
The First Affiliated Hospital of Zhengzhou University
Longyao Ma
The First Affiliated Hospital of Zhengzhou University
Yang Liu
The First Affiliated Hospital of Zhengzhou University
Sha Zhou
The First Affiliated Hospital of Zhengzhou University
Yong Zhang
The First Affiliated Hospital of Zhengzhou University
Weijian Wang
weijianwang520@163.com

The First Affiliated Hospital of Zhengzhou University

Research Article

Keywords:

Posted Date: August 20th, 2026

DOI: https://doi.org/10.21203/rs.3.rs-10477791/v1

License: This work is licensed under a Creative Commons Attribution 4.0 International License.
Read Full License

Additional Declarations: No competing interests reported.

Abstract

Background

Internet gaming disorder (IGD) is a behavioral addiction whose resting-state brain signature may be expressed in transient connectivity configurations rather than in a scan-wide average.

Methods

Resting-state fMRI data from 58 participants with IGD and 56 healthy controls were analysed with Dosenbach-160 regional time series, 60-TR sliding windows, and a four-state k-means solution evaluated by geometric-elbow, repeated-initialisation, split-half, and window-length analyses. State-specific AUC graph metrics and temporal metrics were compared with covariate-adjusted models and residual-permutation inference. Linear SVR with leave-one-out cross-validation tested prediction of Internet Addiction Test (IAT) scores within the IGD group, with repeated nested cross-validation as a robustness analysis.

Results

Under within-state FDR correction, group differences in graph topology were confined to State 4: IGD showed lower clustering, global efficiency, local efficiency, normalised clustering, and small-worldness, together with longer characteristic path length. Local efficiency, normalised clustering, and small-worldness remained significant after correction across all 28 state-by-metric tests. IGD showed lower fractional occupancy and shorter mean dwell time in States 1 and 4 and higher fractional occupancy and longer mean dwell time in State 3 (nine-outcome FDR $q <= 0.024$); State 2 temporal measures and total transitions did not differ. State-specific graph features predicted IAT scores in State 2 ($r = 0.56$, $q = 0.010$, $n = 58$) and State 4 ($r = 0.57$, $q = 0.015$, $n = 45$); repeated nested cross-validation yielded median r values of 0.54 and 0.58, respectively.

Conclusions

IGD was characterised by a state-dependent redistribution of temporal occupancy, together with State 4-specific topological disruption. State-resolved graph features also tracked symptom severity in States 2 and 4. These findings support complementary temporal and topological characterisation of dynamic brain-network alterations in IGD, while requiring replication in larger independent samples.

Background

Internet gaming disorder (IGD) is now widely recognized as a behavioral addiction, and the associated public-health burden is substantial: meta-analytic estimates place the global prevalence near 3%, and the

burden falls disproportionately on adolescents and young men [1]. Population and clinical surveys link the condition to a broad set of risk factors and to escalating functional impairment as symptoms intensify [2]. Clinically, IGD is marked by weakened executive control, heightened sensitivity to gaming-related reward, and persistent craving [3], and in younger cohorts it frequently travels with emotional dysregulation and academic decline [4]. Because these problems rarely resolve on their own and existing treatments remain modest in effect, clarifying the disorder's neural basis has become a priority [5]. A growing consensus holds that the relevant unit of analysis is not any single region but the coordinated activity of large-scale networks, whose disturbed interactions may give rise to the behavioral profile of IGD [6].

Resting-state functional connectivity (rsFC) has been the primary means of charting this network-level disturbance. Work in reward circuitry shows that connectivity between the ventral tegmental area and the nucleus accumbens is weaker in IGD and tracks addiction severity [7]. Frontostriatal pathways that support cognitive control are likewise attenuated, with the degree of reduction scaling with symptom load [8]. Other studies describe a shift in the balance of ventral and dorsal striatal connectivity that parallels the move from recreational to compulsive gaming [9]. Despite this progress, most rsFC studies distil an entire scan into a single connectivity value, an approach that assumes connectivity is stationary across the recording. That assumption is difficult to defend, because connectivity fluctuates over seconds to minutes, and these fluctuations are structured rather than random, carrying information that a single time-averaged estimate cannot recover [10].

Dynamic functional connectivity was developed to preserve exactly this information. By sliding a window along the scan and clustering the resulting connectivity patterns, the method resolves a recording into a small set of recurring, transient states, each with its own spatial signature and temporal properties such as mean dwell time and the number of transitions [11]. In schizophrenia, this framework revealed that dysconnectivity is confined to specific states and largely absent from others, a structure that static analysis had obscured [12, 65]. The same state dependence has since been reported across psychiatric diagnoses [13] and shown to carry cognitive and clinical relevance at the population scale [14]. In IGD the dynamic literature is young but growing: reports describe altered temporal variability of functional networks [15], reduced stability of local connectivity [16], atypical interhemispheric functional connectivity [17], and disrupted cortico-limbic dynamics in adolescent patients [18]. Together they establish that IGD changes how strongly and how variably regions connect within states, yet they leave open how the network is organized inside each state.

That organizational question is the province of graph theory, which recasts the brain as a set of nodes and edges and quantifies the balance between functional segregation and integration [19]. A standard family of measures, including the clustering coefficient, characteristic path length, and global and local efficiency, captures how economically information can be routed across the network [20]. Healthy brains approximate a small-world architecture that couples dense local processing with short global communication, a configuration thought to underlie efficient cognition [21]. Applied to IGD, graph analyses consistently indicate that network topology is abnormal, even though the specific findings are

heterogeneous across studies. Functional-network studies report altered efficiency and clustering at rest [22]. Comparisons with recreational game users, matched on gaming exposure, attribute these differences to the disorder rather than to gaming itself and point to a reorganization of network integration and segregation rather than a wholesale loss of connections [23, 24, 25]. Structural and diffusion-imaging work points in the same direction, reporting altered topology of anatomical connections and disrupted white-matter network organization [26, 27]. What these results share, beyond their inconsistency, is that each is derived from a single static graph spanning the entire scan, which averages over the state structure that dynamic analyses expose.

State-specific graph analysis has uncovered disease effects in major depression that static, time-averaged graphs miss [28], and the transdiagnostic evidence above indicates that such effects are often restricted to particular states [13]. Computing graph topology within each dynamic state, rather than over the whole recording, joins these two literatures and addresses their shared blind spot. In parallel, connectivity is increasingly used not only to contrast groups but to predict individual severity: resting-state features forecast symptom scores in IGD [29], effective-connectivity measures carry predictive value for clinical severity [30], and connectome-based models extend this logic to other addictions such as smoking [31]. Connectivity-defined subtypes of IGD further show that these features index clinically meaningful heterogeneity [32]. Building on these lines, we combined sliding-window dynamic functional connectivity with graph theory in 58 individuals with IGD and 56 healthy controls. Each scan was parsed into several recurring states; within every state we computed area-under-the-curve graph metrics, compared topology between groups, and tested whether state-specific features predict addiction severity on the Internet Addiction Test. We hypothesized that topological disruption in IGD is state-specific rather than pervasive, and that the organization of the affected states scales with clinical severity.

Methods

Participants

We analysed resting-state data from 114 right-handed participants, comprising 58 individuals with internet gaming disorder (IGD) and 56 healthy controls (HC), all recruited from the First Affiliated Hospital of Zhengzhou University. IGD was diagnosed by experienced psychiatrists according to the fifth edition of the Diagnostic and Statistical Manual of Mental Disorders (DSM-5) [33] together with the Internet Addiction Test (IAT) [34]. The IAT is a twenty-item self-report scale, each item rated from 1 to 5, on which higher totals index more compulsive and impairing use. Participants who met at least five DSM-5 criteria and scored 50 or above on the IAT were assigned to the IGD group; HC participants did not meet DSM-5 IGD criteria and were screened below the IAT threshold. Individual HC IAT totals were not retained in the analysis dataset. To reduce the chance of undetected comorbidity, every participant additionally completed a structured clinical interview based on the Mini-International Neuropsychiatric Interview [35]. Individuals were not enrolled if they had a diagnosis of anxiety disorder, major depressive disorder, substance use disorder, or attention-deficit/hyperactivity disorder, and the same applied to

intellectual disability and to any neurological disorder or history of brain injury. Participants were asked to refrain from medication and psychoactive substances on the day of scanning. IAT scores retained for the analysis were therefore available for IGD participants only and were used as the within-IGD severity target. The study was approved by the Ethics Committee of the First Affiliated Hospital of Zhengzhou University (2022-KY-0438) and was conducted in accordance with the Declaration of Helsinki, and all participants gave written informed consent before enrolment. Group demographic and clinical characteristics are summarised in Table 1.

Table 1
Demographic, motion, and IAT characteristics of the HC and IGD groups

Characteristic	HC	IGD	Test	P value	Cohen's d
Sample size, n	56	58	—	—	—
Age, years	15.57 ± 5.51	14.64 ± 1.97	Welch t = 1.20	0.236	−0.23
Education, years	9.07 ± 4.14	8.76 ± 1.81	Welch t = 0.52	0.605	−0.10
Mean framewise displacement, mm	0.169 ± 0.081	0.182 ± 0.067	Welch t = −0.95	0.344	—
Sex, male/female	41/15 (73.2% male)	49/9 (84.5% male)	$\chi^2 = 2.18$	0.140	—
IAT score	NA	79.84 ± 11.50	—	—	—

Note. Continuous variables are presented as mean ± SD. Age, education, and mean framewise displacement were compared using Welch's independent-samples t tests; sex distribution was compared using the chi-square test. Cohen's d is oriented as IGD minus HC. IAT screening was used for HC eligibility, but individual HC IAT totals were not retained in the analysis dataset. The IGD IAT summary corresponds to the target used in the state-specific SVR analysis.

Image acquisition and preprocessing

Imaging was performed on a 3T Siemens MAGNETOM Prisma scanner with a 64-channel head coil. During the resting-state run, participants were asked to stay awake with their eyes closed, remain relaxed, and refrain from any deliberate mental activity, and foam padding and earplugs were used to limit head motion and scanner noise. Functional images were collected with a gradient-echo echo-planar sequence with the following parameters: repetition time 1000 ms, echo time 30 ms, flip angle 70 degrees, field of view 220 x 220 mm2, voxel size 2 x 2 x 2.2 mm3, 52 slices, and 400 volumes.

Image preprocessing was performed using DPARSF [36], which is based on SPM. After conversion from DICOM to NIfTI, the initial five volumes of each run were discarded to allow signal equilibration, leaving 395 volumes per participant. The remaining images underwent slice-timing correction and six-parameter rigid-body realignment. Participants with head motion exceeding 2.5 mm of translation or 2.5 degrees of rotation were excluded. Functional images were then normalised to the standard echo-planar imaging

template, resampled to 3 x 3 x 3 mm3, and spatially smoothed with a 6-mm full-width-at-half-maximum Gaussian kernel. Friston-24 motion parameters and mean white-matter and cerebrospinal-fluid signals were regressed out as nuisance covariates, and linear detrending was applied [37–39, 66]. Mean framewise displacement was retained for each participant as a summary of in-scanner motion and was included as a covariate in every group-level model [38, 39].

Regional time series and sliding-window dynamic functional connectivity

Preprocessed images were parcellated with the Dosenbach-160 atlas, which samples cortical, subcortical, and cerebellar systems and has been widely used in developmental and clinical work [40]. Each region of interest was defined as a small sphere centred on the published coordinates, and a representative time series was extracted for each of the 160 regions by averaging the signal across the voxels within the sphere. Time-varying connectivity was then estimated with a sliding-window approach [10, 11]. A rectangular window spanning 60 repetition times, equivalent to 60 s at this repetition time, was advanced across the scan in steps of 2 repetition times, which produced 168 overlapping windows for each participant. A window of this length is long enough to yield stable correlation estimates yet short enough to track reconfiguration over time, and it sits within the range recommended for dynamic analyses at this repetition time [41]. Within each window we quantified connectivity between every pair of regions with a Pearson correlation and applied a Fisher z-transformation to stabilise the variance, which produced a 160 x 160 matrix per window. The upper triangle of this matrix, comprising 12,720 unique edges, served as the feature vector that described the connectivity pattern of that window. The complete analysis workflow is summarised in Fig. 1.

Connectivity-state clustering

To identify connectivity patterns that recurred across time and participants, the 19,152 window feature vectors were concatenated and submitted to scikit-learn Lloyd k-means clustering with the squared-Euclidean objective [11, 45]. Candidate solutions from K = 2 to K = 10 were evaluated. In the primary full-window analysis, 100 single-initialisation fits were run for each K with fixed random seeds, the lowest-inertia solution was retained, and the elbow was defined by the maximum normalised point-to-line distance from the line joining the K = 2 and K = 10 inertia values. This fixed geometric rule selected K = 4. We then evaluated the dependence of this choice on initialisation and window length. For each 40-, 60-, and 80-s window definition, six windows per participant were selected with a fixed seed, one from each of six equal temporal strata, giving a subject-balanced sample of 684 windows. For every candidate K, 150 single-initialisation fits were run with a maximum of 500 iterations, and the elbow was evaluated on both the best- and median-inertia curves and across matched initialisation curves. Stability of the K = 4 solution was further assessed in 100 group-stratified split-half resamples, using ten starts per half; centroids were matched with the Hungarian algorithm and compared using Pearson correlations. The 60-s sampled centroids were also matched to the primary full-window centroids, and centroids were compared across window lengths. Because these analyses supported K = 4 at the aggregate level but did not establish it as uniquely optimal, K = 4 was retained as a literature-comparable higher-resolution

solution. State numbers were the primary k-means labels shifted from zero-based to one-based indexing, without outcome-based relabelling. Each window was assigned to its cluster centroid, and, for every participant and state, the window-wise matrices belonging to that state were averaged to give a subject-specific mean connectivity matrix for graph analysis.

Temporal properties of connectivity states

Three temporal measures were derived from each participant's ordered sequence of 168 state labels. Fractional occupancy was the proportion of windows assigned to each state, mean dwell time was the average number of consecutive windows spent in that state per visit, and total transitions was the number of switches between adjacent labels across the run. Fractional occupancy was zero when a participant did not express a state; mean dwell time was undefined for an unexpressed state and was left missing rather than set to zero or imputed. Fractional occupancy and total transitions therefore included all 114 participants, whereas state-specific mean dwell time included only state expressers (State 1, n = 50; State 2, n = 110; State 3, n = 105; State 4, n = 85). State-specific graph and prediction analyses likewise remained restricted to participants with an observed subject-state connectivity matrix.

State-specific graph-theoretical analysis

Graph-theoretical metrics were computed for each subject-state mean matrix in the GRETNA toolbox [44]. Self-connections were removed and negative correlations were set to zero. Rather than fix a single connection density, we binarised each matrix across network sparsities from 0.03 to 0.40 in steps of 0.01, which keeps the number of edges comparable across participants and reduces dependence on any one threshold [43]. At every sparsity we computed the clustering coefficient and local efficiency, which index functional segregation, together with characteristic path length and global efficiency, which index functional integration. GRETNA's harmonic formulation was used for path-length calculations in disconnected graphs. We also computed the normalised clustering coefficient and normalised characteristic path length against 20 degree-matched random networks and combined them into small-worldness [20, 21, 42]. The original batch analysis did not set an explicit random-number seed for random-network generation. Nodal degree and nodal efficiency were computed at each of the 160 nodes [63]. Values across the sparsity range were integrated into area-under-the-curve summaries, giving the global measures aCp, aEg, aEloc, aLp, aGamma, aLambda, and aSigma and the nodal measures aNodalDegree and aNodalEfficiency.

Statistical analysis

Analyses were carried out in Python. Age, years of education, and mean framewise displacement were compared between groups with Welch's independent-samples t tests, with Cohen's d (oriented as IGD minus HC) reported for age and education, and sex distribution was compared with a chi-square test; results appear in Table 1. IAT scores were summarised descriptively and used as the within-IGD severity target.

Graph-theoretical metrics were analysed with a general linear model. For each area-under-the-curve metric we fitted a model that included group, sex, age, education, and mean framewise displacement, with HC coded as 0 and IGD as 1, and evaluated the group term with a two-tailed t test at an alpha of 0.05. For global metrics, the prespecified primary Benjamini-Hochberg false-discovery-rate (FDR) correction was applied within each state across the seven measures; an additional Benjamini-Hochberg FDR sensitivity correction was applied across all 28 state-by-metric tests. All nodal p values from the four states, two nodal measures, and 160 nodes (4 x 2 x 160 = 1,280 tests) were included in one prespecified family and corrected using the Benjamini-Hochberg FDR procedure. An FDR-adjusted $q < 0.05$ defined statistical significance. State labels were retained from the fixed clustering solution and were not assigned according to statistical significance.

Temporal outcomes were analysed with general linear models containing group, sex, age, education, and mean framewise displacement, with HC coded as 0 and IGD as 1. Fractional occupancy and mean dwell time were tested separately for each state, and total transitions was tested once, yielding nine group-level outcomes. Ordinary-least-squares estimates, t statistics, and residual degrees of freedom were retained. Inference for the group term used 10,000 two-sided Freedman-Lane residual permutations under the covariate-only reduced model, followed by Benjamini-Hochberg FDR correction across the nine permutation p values. Fractional-occupancy and transition models included all 114 participants (residual df = 108); mean-dwell-time models used state expressers only, with residual df = 44, 104, 99, and 79 for States 1–4, respectively.

Prediction of symptom severity

Finally, we asked whether state-specific graph topology tracked addiction severity. IAT scores were predicted within the IGD group separately for each state, without selecting a state on the basis of the group comparison. The predictors were five AUC-integrated global measures (aCp, aEg, aEloc, aLp, and aSigma) from IGD participants who expressed the state; aGamma and aLambda were excluded to limit redundancy with aSigma. The primary model was linear support vector regression with L2 regularisation (C = 1.0; epsilon = 0.1) evaluated by leave-one-out cross-validation [45]. Within every fold, covariate models for both the graph features and IAT target were fitted using training participants only, with age, sex, education, and mean framewise displacement as covariates. Training features and targets were residualised, held-out features were residualised using training coefficients, the held-out covariate-predicted IAT offset was added back to the residual prediction, and feature standardisation was fitted within the training fold. Performance was quantified by Pearson r, cross-validated Q2, mean absolute error, and root-mean-square error. Significance used 5,000 two-sided Freedman-Lane reduced-model residual permutations, each repeating the complete leave-one-out pipeline; the four state-level p values were corrected together by Benjamini-Hochberg FDR. As a robustness analysis, we repeated nested five-fold cross-validation 100 times, using four-fold inner cross-validation to select C from 0.01, 0.1, 1, 10, and 100 and epsilon from 0.01, 0.1, 0.5, 1, and 2 by inner-fold root-mean-square error. Covariate adjustment and scaling were refitted within every inner and outer training set. Robustness results were

summarised by the median and 2.5th-97.5th percentiles across repeats. Full specifications are provided in Table S6.

Results

Sample characteristics

Mean age did not differ between HC and IGD under Welch's test (15.57 ± 5.51 versus 14.64 ± 1.97 years; t = 1.20, df = 68.4, p = 0.236, Cohen's d = − 0.23), nor did years of education (9.07 ± 4.14 versus 8.76 ± 1.81 years; t = 0.52, df = 74.7, p = 0.605, d = − 0.10), mean framewise displacement (0.169 ± 0.081 versus 0.182 ± 0.067 mm; p = 0.344), or sex distribution (41/15 versus 49/9 male/female; $\chi^2 = 2.18$, p = 0.140). These null mean comparisons were not interpreted as evidence that the distributions were equivalent. IAT screening was used during HC eligibility assessment, but individual HC IAT totals were not retained in the analysis dataset. The mean IAT score among the 58 IGD participants was 79.84 ± 11.50. Sample characteristics are reported in Table 1.

Dynamic connectivity states

Concatenating the 168 windows from each of the 114 participants yielded 19,152 sliding-window connectivity matrices. The fixed point-to-line rule selected K = 4 from the primary full-window inertia curve. In the subject-balanced 150-start analysis, the median-inertia elbow was K = 4 at 40, 60, and 80 s, whereas the best-inertia curve selected K = 5 at 40 and 80 s; K = 4 was nevertheless the modal initialization-level elbow at each window length (54.7%, 66.7%, and 45.3%, respectively). The four 60-s sampled centroids closely matched the full-window centroids (r = 0.988–0.993). Across 100 split-half repetitions, the median matched-centroid correlation was 0.894 (2.5th-97.5th percentile, 0.351–0.920), although 15 repetitions contained one centroid with r < 0.50. Cross-window matching was high for all 40-s centroids and three of four 80-s centroids (r = 0.950–0.989), while one 80-s centroid was less stable (r = 0.373). K = 4 was therefore retained as a literature-comparable higher-resolution solution rather than claimed as uniquely optimal (Table S1, Figure S1). State numbers were retained directly from this fixed solution. Seventy-two participants did not express at least one state, yielding 106 missing subject-by-state matrices; these cells were not imputed (Table S2). Figure 2 displays the state-centroid matrices and temporal profiles derived from the ordered state sequences. State 1 accounted for 10.0% of all windows (1,916 windows), was expressed by 50 participants, and showed the strongest connectivity (mean within-network Fisher z = 0.62, between-network Fisher z = 0.53). State 2 accounted for 31.1% (5,965 windows), was expressed by 110 participants, and showed intermediate connectivity (within-network Fisher z = 0.29, between-network Fisher z = 0.20). State 3 was the most frequent, accounting for 39.9% (7,651 windows), was expressed by 105 participants, and showed the weakest connectivity (within-network Fisher z = 0.18, between-network Fisher z = 0.10). State 4 accounted for 18.9% (3,620 windows), was expressed by 85 participants, and showed moderately strong connectivity (within-network Fisher z = 0.43, between-network Fisher z = 0.34); 45 of the 85 participants expressing State 4 belonged to the IGD group.

Temporal properties of the connectivity states

Freedman-Lane residual-permutation inference and Benjamini-Hochberg correction across the nine temporal outcomes showed that the IGD group had lower fractional occupancy and shorter mean dwell time in State 1 ($q = 0.011$ and $q < 0.001$) and State 4 ($q = 0.024$ and $q < 0.001$), and higher fractional occupancy and longer mean dwell time in State 3 ($q = 0.002$ and $q = 0.017$). State 2 fractional occupancy and mean dwell time did not differ ($q = 0.898$ and $q = 0.967$), nor did total transitions ($q = 0.530$; Table 2 and Fig. 2). Mean dwell time was evaluated only among participants expressing the corresponding state.

Table 2
Temporal metrics across the four connectivity states

State	Metric	HC, mean ± SD	IGD, mean ± SD	β (IGD − HC)	t	Permutation P	FDR q
1	Fractional occupancy	0.129 ± 0.177	0.072 ± 0.103	−0.075	−2.824	0.005	0.011
1	Mean dwell time (windows)	10.943 ± 2.240	6.030 ± 1.326	−4.898	−9.096	< 0.001	< 0.001
2	Fractional occupancy	0.312 ± 0.169	0.311 ± 0.155	−0.008	−0.260	0.798	0.898
2	Mean dwell time (windows)	12.157 ± 2.491	12.058 ± 2.469	0.018	0.038	0.967	0.967
3	Fractional occupancy	0.341 ± 0.254	0.456 ± 0.212	0.151	3.522	< 0.001	0.002
3	Mean dwell time (windows)	27.105 ± 40.896	38.020 ± 14.763	15.349	2.567	0.009	0.017
4	Fractional occupancy	0.218 ± 0.175	0.161 ± 0.125	−0.068	−2.404	0.016	0.024
4	Mean dwell time (windows)	10.479 ± 2.011	6.863 ± 1.414	−3.553	−9.277	< 0.001	< 0.001
All	Total transitions	12.214 ± 4.159	12.017 ± 4.726	−0.696	−0.824	0.412	0.530

Note. FO, fractional occupancy; MDT, mean dwell time. Values are mean ± SD. Models adjusted for group, sex, age, education, and mean framewise displacement. FO and run-wide transitions included all 114 participants (56 HC, 58 IGD; df = 108). MDT was defined only among state expressers: State 1, n = 50 (22 HC/28 IGD; df = 44); State 2, n = 110 (52/58; df = 104); State 3, n = 105 (53/52; df = 99); State 4, n = 85 (40/45; df = 79). P values are from 10,000 two-sided Freedman–Lane residual permutations; Benjamini–Hochberg FDR was applied across all nine outcomes. The State 3 HC dispersion retains four participants assigned to State 3 for all 168 windows; no observation was trimmed or imputed.

State-specific graph topology

Within-state corrected global graph differences were observed only in State 4; no metric in States 1–3 survived the corresponding seven-metric correction (Table S3 and Figure S2). Among the 85 participants expressing State 4 (df = 79), IGD was associated with lower clustering coefficient (0.212 ± 0.006 versus 0.215 ± 0.007; β = −0.003, t = − 2.30, p = 0.024, q = 0.028), global efficiency (0.159 ± 0.013 versus 0.165 ± 0.011; t = − 2.65, p = 0.010, q = 0.017), local efficiency (0.248 ± 0.011 versus 0.255 ± 0.011; t = − 3.28, p = 0.002, q = 0.006), normalised clustering γ (0.455 ± 0.054 versus 0.499 ± 0.090; t = − 3.13, p = 0.002, q =

0.006), and small-worldness σ (0.433 ± 0.048 versus 0.471 ± 0.077; t = − 3.09, p = 0.003, q = 0.006), together with longer characteristic path length (1.036 ± 0.123 versus 0.984 ± 0.101; β = 0.058, t = 2.41, p = 0.018, q = 0.026). Normalised path length λ did not differ (p = 0.180). Under the sensitivity correction across all 28 state-by-metric tests, aEloc, aGamma, and aSigma remained significant (all q = 0.026), whereas aCp, aEg, and aLp did not (q = 0.114, 0.068, and 0.103, respectively). At the nodal level, no effect survived Benjamini-Hochberg FDR correction across the prespecified family of all 1,280 tests (minimum q = 0.223; Table S4). State 4 global results are reported in Table 3.

Table 3
State 4 global graph-theoretical metrics by group

Metric	HC, mean ± SD	IGD, mean ± SD	β (IGD − HC)	t	df	P	FDR q (state)
aCp	0.215 ± 0.007	0.212 ± 0.006	−0.003	−2.295	79	0.024	0.028
aEg	0.165 ± 0.011	0.159 ± 0.013	−0.007	−2.653	79	0.010	0.017
aEloc	0.255 ± 0.011	0.248 ± 0.011	−0.008	−3.283	79	0.002	0.006
aLp	0.984 ± 0.101	1.036 ± 0.123	0.058	2.406	79	0.018	0.026
aGamma	0.499 ± 0.090	0.455 ± 0.054	−0.050	−3.133	79	0.002	0.006
aLambda	0.390 ± 0.011	0.387 ± 0.010	−0.003	−1.352	79	0.180	0.180
aSigma	0.471 ± 0.077	0.433 ± 0.048	−0.043	−3.091	79	0.003	0.006

Note. Values are mean ± SD. State 4 complete cases were n = 85 (40 HC, 45 IGD; df = 79). Group effects were estimated using GLM: metric ~ group + sex + age + education + mean framewise displacement. β represents IGD minus HC. Global metrics are AUC-integrated over sparsity 0.03–0.40. The table reports FDR q values across the seven metrics within State 4. In the sensitivity correction across all 28 state-by-metric tests, aEloc, aGamma, and aSigma remained significant (all q = 0.026); aCp, aEg, and aLp had q = 0.114, 0.068, and 0.103, respectively. HC, healthy controls; IGD, Internet gaming disorder.

Prediction of addiction severity

State-specific graph features were used to predict IAT scores within IGD, with graph features and the IAT target adjusted for age, sex, education, and mean framewise displacement within every training fold. Prediction survived four-state FDR in State 2 (r = 0.559, Freedman-Lane p = 0.0024, q = 0.0096, Q^2 = 0.265, mean absolute error 7.94, root-mean-square error 9.77, n = 58) and State 4 (r = 0.566, p = 0.0074, q = 0.0148, Q^2 = 0.310, mean absolute error 7.49, root-mean-square error 9.40, n = 45). State 1 (r = 0.249, q

= 0.558, n = 28) and State 3 (r = 0.354, q = 0.201, n = 52) did not survive correction. Across 100 repetitions of nested cross-validation, State 2 had median r = 0.538 (2.5th-97.5th percentile, 0.436–0.597) and median Q^2 = 0.215, while State 4 had median r = 0.581 (0.470–0.662) and median Q^2 = 0.300. By contrast, median Q^2 remained negative in States 1 and 3 (-0.339 and − 0.042). Figure 3 shows the primary State 2 and State 4 models; Table S5 and Figure S3 report the complete primary and nested-validation results, and Table S6 provides the analysis specification.

Discussion

We combined sliding-window dynamic functional connectivity with graph theory to test whether the network disturbance of internet gaming disorder (IGD) is a pervasive property of the resting brain or a feature of specific transient configurations. Three findings define the central advance. First, group differences in graph topology were confined to a single connectivity state, State 4, and were absent from the other three, so IGD did not present as a pervasive, scan-wide network deficit. Second, the IGD group also occupied the more strongly connected states less often than controls, so the affected configuration was both entered less frequently and organised less efficiently once entered. Third, the topology of that same state tracked addiction severity within the IGD group. Read together, these results recast IGD as a state-specific rather than a pervasive network disorder [12, 28], consistent with the transdiagnostic observation that dysconnectivity is often restricted to particular states [13], and they show that a network account of the disorder benefits from resolving connectivity in time rather than averaging over it [46].

State occupancy links network dynamics to behaviour

The temporal findings connect the dynamics of state visitation to the behavioural profile of the disorder. The IGD group spent less time in, and dwelled more briefly within, the strongly connected States 1 and 4 and instead lingered in the weakly connected State 3, whereas the number of transitions was unchanged. A bias away from strongly integrated configurations toward a low-connectivity regime would be consistent with the weakened executive control [47] and reward-driven disengagement [48] that characterise addiction, in which the balance between a hypoactive reflective system and a hypersensitive reward system is thought to shift toward the latter [49, 50]. Because resting activity is organised as metastable transitions among recurring configurations rather than as a fixed pattern [51], spending less time in integrative states may index a reduced capacity to sustain the coordinated processing that goal-directed control requires, and the corresponding preference for a weakly connected, default-like regime echoes the default-mode dominance reported across addictions [52]. Beyond how often each configuration is entered, however, the more decisive question concerns what happens inside a state once it is occupied.

A coherent, state-confined disruption of network topology

That within-state organisation is where the disorder left its clearest mark. Within State 4 the disruption was strikingly coherent: six of the seven global metrics survived the prespecified within-state correction

and moved together in IGD. Local efficiency, normalised clustering, and small-worldness also remained significant under the sensitivity correction across all 28 state-by-metric tests. The clustering coefficient and local efficiency, which index functional segregation, were reduced; the global efficiency was reduced and the characteristic path length lengthened, both indexing weaker functional integration; and the normalised clustering and small-worldness fell in step. Rather than a selective loss of either segregation or integration, this pattern describes a simultaneous erosion of both, that is, a drift away from the economical small-world organisation that supports efficient information transfer at low wiring cost [53]. Because the healthy brain is thought to hold segregation and integration in a fine balance [54], and because that balance configures cognitive capacity [55], a coordinated reduction across metrics is a more plausible signature of a disorder than any single deviating index, and it aligns with the view of psychiatric conditions as disturbances of connectome-level organisation [56]. Critically, these changes all ran in the same direction. Reduced clustering and local efficiency, reduced global efficiency, a longer characteristic path length, and lower small-worldness together describe a network that communicates and integrates information less efficiently than that of controls [20, 53]. Because a longer path length and lower efficiency imply that signalling between distant regions must take less direct routes, the long-range, coordinated integration on which controlled behaviour depends becomes harder to sustain [55]. This reduced efficiency offers a candidate substrate for the behavioural profile of IGD, which is marked by weakened inhibitory and executive control and heightened reward sensitivity [3] and in which behavioural meta-analyses have repeatedly confirmed impaired response inhibition [57]. A network that integrates information less efficiently precisely when goal-directed control is demanded is a plausible correlate of exactly these deficits, so a state in which segregation and integration are jointly reduced is the configuration one would expect to accompany the disorder's control failures rather than an incidental abnormality. Locating this effect inside one transient state also offers a parsimonious account of why previous static graph studies of IGD have reported abnormal yet mutually inconsistent topology [22, 26, 27]: a single graph spanning the whole scan mixes State 4 with three states in which topology is preserved, diluting and sometimes reversing the effect, the kind of heterogeneity that meta-analyses of the IGD literature have repeatedly encountered [58, 59].

Temporal and topological effects converge on one configuration

Beyond confirming the state-specific account, the two findings together invite a stronger interpretation of what that account implies. Network abnormality in addiction has typically been framed either as a pervasive reorganisation of the resting brain or as a redistribution of time across states; the present pattern fits neither, because the temporal differences were distributed across several states whereas the topological disruption was confined to State 4. This dissociation suggests that the disorder's signature resides less in how often each configuration is visited than in how one particular configuration is internally organised. On this reading, IGD may be characterised as a state-specific rather than a whole-brain disturbance: the repertoire of connectivity states is broadly preserved, and the abnormality is expressed transiently, only while the affected integrative configuration is occupied. The convergence supports this view, because State 4 was the single state that was entered less often, organised less efficiently once entered, and predictive of symptom severity; the temporal effects may therefore be a

comparatively non-specific correlate, whereas the topological failure of this integrative state may be closer to the core of the disorder. Selective involvement of one integrative regime, rather than of an isolated region or of global connectivity, is consistent with models that attribute addiction to disturbed interaction among large-scale control, salience, and reward networks [60, 61], and it accounts for the difficulty of detecting the effect with static, time-averaged analyses, which average State 4 together with the other states and with the temporal structure that isolates it [10, 11]. If the interpretation is borne out, it also reframes the target of intervention: rather than normalising connectivity globally, treatment might aim to restore the efficient organisation of State 4 or to promote its adequate engagement, with State 4 topology serving as a state-resolved marker for patient stratification and for monitoring change. These possibilities are necessarily tentative and require longitudinal and interventional confirmation, but they follow directly from localising the disturbance to a single transient state.

State-specific topology tracks addiction severity

The clinical relevance of the affected topology is reinforced by the prediction analysis. State-specific graph features predicted Internet Addiction Test scores within the IGD group in two states, and, because the four states were tested separately with correction across states, this result was obtained without preselecting a state on the group difference and is therefore free of circularity. State 2 and State 4 also retained positive median cross-validated Q2 and similar median correlations across 100 repetitions of nested cross-validation, while States 1 and 3 retained negative median Q2; this separation argues against the result being an idiosyncrasy of a single leave-one-out partition or fixed regularisation setting, although the State 2 Q2 distribution included some negative repetitions. That the predictive set included State 4, the same state in which topology differed between groups, means the configuration is not only altered on average but also scales with symptom load, linking a categorical group effect to a dimensional brain-behaviour relationship. State 2, the most widely expressed state, also predicted severity without showing a group difference, a reminder that severity-relevant variation need not coincide with a mean group shift. These results extend a growing body of work showing that resting connectivity forecasts symptom severity in IGD [29, 30] and in other addictions [31], and that connectivity features index clinically meaningful heterogeneity [32], and they are consistent with the engagement of these networks during gaming cue reactivity [62].

Implications for dynamic and stratified IGD research

Two implications follow for how IGD is studied. First, because the disorder's topological signature was carried by a single transient configuration, analyses that average over an entire scan are likely to under-detect it, and dynamic, state-resolved designs should be preferred when the question concerns network organisation rather than overall connection strength. Second, the convergence of a group difference and a severity association on the same state suggests that State 4 topology is a candidate marker for stratifying patients and for tracking change, provided its origin is first clarified. A process-based view of addictive behaviour, in which affective, cognitive, and executive components interact and evolve as the disorder develops [50], motivates longitudinal and treatment-outcome designs that would test whether

the State 4 abnormality precedes, accompanies, or follows escalating symptoms, and whether connectivity-defined heterogeneity [32] maps onto the state-specific pattern reported here. These are directions for research rather than clinical recommendations.

Limitations

Several considerations frame the interpretation of these findings. First, the cross-sectional, single-site design does not establish whether the State 4 pattern precedes the development of IGD, emerges with illness progression, or reflects a correlate of current symptom burden. Replication in larger, multisite longitudinal samples will therefore be important, particularly because the present cohort was predominantly male, covered a relatively broad age range, and showed incomplete overlap in the age distributions of the two groups. These features limit the extent to which the present estimates can be generalised to females, narrower developmental periods, and other clinical or cultural settings.

Second, the state-specific analyses necessarily apply to participants who expressed the relevant state. State 4 was not observed in 29 participants, and the corresponding graph and prediction analyses were therefore based on smaller state-expressing subsets; no minimum number of State 4 windows was imposed beyond state expression. The findings should consequently be interpreted as characterising the topology of an expressed configuration rather than as demonstrating that every individual with IGD shows the same state-specific alteration.

Third, connectivity-state solutions remain conditional on analytic choices. Although the four-state solution was supported by the full-window geometric criterion, analyses across window lengths and initialisations, and split-half centroid matching, alternative parameterisations did not identify K = 4 as uniquely optimal in every instance. The broad state-level pattern was nevertheless reproducible across the prespecified sensitivity analyses, whereas the precise numbering and fine-grained identity of individual centroids should not be regarded as definitive. Future work should test whether comparable state-resolved effects are recovered with independent samples, parcellations, and dynamic-connectivity models.

Finally, the prediction analyses provide internal rather than external validation. Repeated nested cross-validation and permutation testing reduce dependence on a particular data split, but they cannot substitute for prospective replication in an independent IGD cohort. In addition, IAT scores were available only within the IGD group, and no nodal effect survived correction across the full nodal testing family. The present results therefore support a network-level association between state-specific topology and symptom severity, but do not yet establish a node-level substrate or a clinically deployable biomarker.

Conclusions

In summary, the resting brain in IGD is not disorganised in a pervasive, scan-wide manner. Its topological disruption is confined to a single transient connectivity state, in which functional segregation, functional integration, and small-worldness decline together, and the same strongly connected configuration is

entered less often and maintained for less time. The topology of that state scales with addiction severity, linking a categorical group difference to a dimensional brain-behaviour relationship. Taken together, these results support a state-resolved, graph-based view of IGD, while making clear that longitudinal follow-up, network-level localisation, and replication in larger and more diverse samples are needed before the state-specific pattern can be interpreted mechanistically or used clinically.

Abbreviations

aCp: area under the curve of clustering coefficient; aEg: area under the curve of global efficiency; aEloc: area under the curve of local efficiency; aGamma: area under the curve of normalised clustering coefficient; aLambda: area under the curve of normalised characteristic path length; aLp: area under the curve of characteristic path length; aSigma: area under the curve of small-worldness; AUC: area under the curve; DICOM: Digital Imaging and Communications in Medicine; DPARSF: Data Processing & Analysis for (Resting-State) fMRI; DSM-5: Diagnostic and Statistical Manual of Mental Disorders, Fifth Edition; FDR: false discovery rate; fMRI: functional magnetic resonance imaging; FO: fractional occupancy; GRETNA: Graph Theoretical Network Analysis; HC: healthy controls; IAT: Internet Addiction Test; IGD: internet gaming disorder; LOOCV: leave-one-out cross-validation; MDT: mean dwell time; MINI: Mini-International Neuropsychiatric Interview; MRI: magnetic resonance imaging; NIfTI: Neuroimaging Informatics Technology Initiative; rsFC: resting-state functional connectivity; SD: standard deviation; SPM: Statistical Parametric Mapping; SVR: support vector regression; TR: repetition time

Declarations

Ethics approval and consent to participate

This study was approved by the Ethics Committee of the First Affiliated Hospital of Zhengzhou University (approval number: 2022-KY-0438) and was conducted in accordance with the Declaration of Helsinki. Written informed consent was obtained from all participants prior to enrolment.

Consent for publication

Not applicable.

Availability of data and materials

The datasets generated and/or analysed during the current study are not publicly available due to participant privacy considerations but are available from the corresponding author on reasonable request.

Competing Interests

The authors declare no competing interests.

Funding

This work was supported by the Henan Provincial Medical Science and Technology Research Project Major Project Jointly Established by Provincial and Ministerial Authorities (No. SBGJ202101013), the Key Research Project Program for Higher Education Institutions in Henan Province in 2024 (No. 24A320059), the National Natural Science Foundation of China (No. 82471962), and the Special Project for Scientific Research on Traditional Chinese Medicine in Henan Province in 2024 (No. 2024ZY3085).

Authors' contributions

Yichen Guo: Conceptualization, Methodology, Formal analysis, Data curation, Visualization, Writing - original draft. Guohao Lu: Methodology, Investigation, Data curation. Xinyu Wang: Methodology, Investigation, Writing - review & editing. Wenjing Li: Investigation, Data curation. Longyao Ma: Investigation, Data curation. Yang Liu: Investigation, Data curation. Sha Zhou: Investigation, Data curation. Yong Zhang: Resources, Supervision, Project administration, Writing - review & editing. Weijian Wang: Conceptualization, Funding acquisition, Supervision, Writing - review & editing, Correspondence.

Acknowledgements

Not applicable.

References

1. Stevens MW et al. Global prevalence of gaming disorder: A systematic review and meta-analysis. Aust N Z J Psychiatry. 2021. PMID 33028074.
2. Gao YX et al. Prevalence and possible risk factors of internet gaming disorder: meta-analyses. J Psychiatr Res. 2022. PMID 35926424.
3. Weinstein A, Lejoyeux M. Neurobiological mechanisms underlying internet gaming disorder. Dialogues Clin Neurosci. 2020. PMID 32699511.
4. Gentile DA et al. Internet Gaming Disorder in Children and Adolescents. Pediatrics. 2017. PMID 29093038.
5. Paulus FW et al. Internet gaming disorder in children and adolescents: a systematic review. Dev Med Child Neurol. 2018. PMID 29633243.
6. Yan H et al. Large-scale network dysfunction in youths with internet gaming disorder: a meta-analysis of resting-state functional connectivity studies. Prog Neuropsychopharmacol Biol Psychiatry. 2021. PMID 33434637.
7. Wang R et al. Internet gaming disorder: deficits in functional and structural connectivity in the ventral tegmental area-accumbens pathway. Brain Imaging Behav. 2019. PMID 30054871.

8. Dong H et al. Reduced frontostriatal functional connectivity and associations with severity of internet gaming disorder. Addict Biol. 2021. PMID 33236526.
9. Dong GH et al. Dorsal and ventral striatal functional connectivity shifts in internet gaming disorder. Commun Biol. 2021. PMID 34262129.
10. Hutchison RM et al. Dynamic functional connectivity: promise, issues, and interpretations. NeuroImage. 2013. PMID 23707587.
11. Allen EA et al. Tracking whole-brain connectivity dynamics in the resting state. Cereb Cortex. 2014. PMID 23146964.
12. Damaraju E et al. Dynamic functional connectivity analysis reveals transient states of dysconnectivity in schizophrenia. NeuroImage Clin. 2014. PMID 25161896.
13. Li C et al. Transdiagnostic time-varying dysconnectivity across major psychiatric disorders. Hum Brain Mapp. 2021. PMID 33210798.
14. Fu Z et al. Cognitive and psychiatric relevance of dynamic functional connectivity states in a large (N > 10,000) children population. Mol Psychiatry. 2025. PMID 39085394.
15. Fu J et al. Temporal variability-based alterations in dynamic functional networks in internet gaming disorder. J Psychiatr Res. 2025. PMID 40334458.
16. Niu X et al. Static and dynamic changes of intrinsic brain local connectivity in internet gaming disorder. BMC Psychiatry. 2023. PMID 37558974.
17. Ma L et al. Alterations in interhemispheric and intrahemispheric functional connectivity dynamics in internet gaming disorder. J Affect Disord. 2025. PMID 39419186.
18. Zhao T et al. Dynamic functional connectivity of the amygdala-hippocampal complex in adolescents with internet gaming disorder. Front Psychiatry. 2025. PMID 41383994.
19. Bullmore E, Sporns O. Complex brain networks: graph theoretical analysis of structural and functional systems. Nat Rev Neurosci. 2009. PMID 19190637.
20. Rubinov M, Sporns O. Complex network measures of brain connectivity: uses and interpretations. NeuroImage. 2010. PMID 19819337.
21. Watts DJ, Strogatz SH. Collective dynamics of 'small-world' networks. Nature. 1998. PMID 9623998.
22. Wang L et al. Altered brain functional networks in people with internet gaming disorder: evidence from resting-state fMRI. Psychiatry Res Neuroimaging. 2016. PMID 27447451.
23. Chen S et al. A preliminary study of disrupted functional network in individuals with internet gaming disorder relative to recreational game users. Addict Behav. 2020. PMID 31801105.
24. Wang Z et al. Cortical thickness and volume abnormalities in internet gaming disorder: evidence from comparison of recreational internet game users. Eur J Neurosci. 2018. PMID 29883011.
25. Wang M et al. Disrupted dynamic network reconfiguration of the executive and reward networks in internet gaming disorder. Psychol Med. 2023. PMID 36004801.
26. Park CH et al. Alterations in the connection topology of brain structural networks in internet gaming disorder. Sci Rep. 2018. PMID 30310094.

27. Zhai J et al. The topological organization of white matter network in internet gaming disorder individuals. Brain Imaging Behav. 2017. PMID 27815774.
28. Zhi D et al. Aberrant dynamic functional network connectivity and graph properties in major depressive disorder. Front Psychiatry. 2018. PMID 30108526.
29. Ye S et al. Predicting the severity of internet gaming disorder with resting-state brain features: a multi-voxel pattern analysis. J Affect Disord. 2022. PMID 36031000.
30. Guo Y et al. Altered effective connectivity in internet gaming disorder and its predictive value for clinical severity: a spectral DCM study. Brain Res Bull. 2026. PMID 42341846.
31. Lin X et al. Connectome-based predictive modelling of smoking severity in smokers. Addict Biol. 2022. PMID 36301219.
32. Wang ZL et al. Subgroups of internet gaming disorder based on addiction-related resting-state functional connectivity. Addiction. 2023. PMID 36089824.
33. American Psychiatric Association. Diagnostic and Statistical Manual of Mental Disorders (DSM-5). 5th ed. Arlington, VA: American Psychiatric Publishing; 2013.
34. Young KS. Internet addiction: the emergence of a new clinical disorder. Cyberpsychol Behav. 1998;1(3):237–44. 10.1089/cpb.1998.1.237.
35. Sheehan DV et al. The Mini-International Neuropsychiatric Interview (M.I.N.I.): the development and validation of a structured diagnostic psychiatric interview for DSM-IV and ICD-10. J Clin Psychiatry. 1998. PMID 9881538.
36. Yan C, Zang Y. DPARSF: a MATLAB toolbox for pipeline data analysis of resting-state fMRI. Front Syst Neurosci. 2010. PMID 20577591.
37. Friston KJ, Williams S, Howard R, Frackowiak RSJ, Turner R. Movement-related effects in fMRI time-series. Magn Reson Med. 1996. PMID 8699946.
38. Power JD et al. Spurious but systematic correlations in functional connectivity MRI networks arise from subject motion. NeuroImage. 2012. PMID 22019881.
39. Satterthwaite TD et al. Impact of in-scanner head motion on multiple measures of functional connectivity. NeuroImage. 2012. PMID 22233733.
40. Dosenbach NUF et al. Prediction of individual brain maturity using fMRI. Science. 2010. PMID 20829489.
41. Leonardi N, Van De Ville D. On spurious and real fluctuations of dynamic functional connectivity during rest. NeuroImage. 2015. PMID 25234118.
42. Humphries MD, Gurney K. Network 'small-world-ness': a quantitative method for determining canonical network equivalence. PLoS ONE. 2008. PMID 18446219.
43. Achard S, Bullmore E. Efficiency and cost of economical brain functional networks. PLoS Comput Biol. 2007. PMID 17274684.
44. Wang J et al. GRETNA: a graph theoretical network analysis toolbox for imaging connectomics. Front Hum Neurosci. 2015. PMID 26175682.

45. Pedregosa F, et al. Scikit-learn: machine learning in Python. J Mach Learn Res. 2011;12:2825–30.
46. Bassett DS, Sporns O. Network neuroscience. Nat Neurosci. 2017. PMID 28230844.
47. Goldstein RZ, Volkow ND. Dysfunction of the prefrontal cortex in addiction: neuroimaging findings and clinical implications. Nat Rev Neurosci. 2011. PMID 22011681.
48. Koob GF, Volkow ND. Neurobiology of addiction: a neurocircuitry analysis. Lancet Psychiatry. 2016. PMID 27475769.
49. Zilverstand A et al. Neuroimaging impaired response inhibition and salience attribution in human drug addiction: a systematic review. Neuron. 2018. PMID 29879391.
50. Brand M et al. The Interaction of Person-Affect-Cognition-Execution (I-PACE) model for addictive behaviors. Neurosci Biobehav Rev. 2019. PMID 31247240.
51. Deco G, Jirsa VK, McIntosh AR. Emerging concepts for the dynamical organization of resting-state activity in the brain. Nat Rev Neurosci. 2011. PMID 21170073.
52. Zhang R, Volkow ND. Brain default-mode network dysfunction in addiction. NeuroImage. 2019. PMID 31229660.
53. Bullmore E, Sporns O. The economy of brain network organization. Nat Rev Neurosci. 2012. PMID 22498897.
54. Sporns O. Network attributes for segregation and integration in the human brain. Curr Opin Neurobiol. 2013. PMID 23294553.
55. Wang R et al. Segregation, integration, and balance of large-scale resting brain networks configure different cognitive abilities. Proc Natl Acad Sci U S A. 2021. PMID 34074762.
56. Fornito A, Zalesky A, Breakspear M. The connectomics of brain disorders. Nat Rev Neurosci. 2015. PMID 25697159.
57. Argyriou E et al. Response inhibition and internet gaming disorder: a meta-analysis. Addict Behav. 2017. PMID 28264786.
58. Niu X et al. Meta-analysis of structural and functional brain alterations in internet gaming disorder. Front Psychiatry. 2022. PMID 37033880.
59. Gao X et al. Structural and functional brain abnormalities in internet gaming disorder and attention-deficit/hyperactivity disorder: a comparative meta-analysis. Front Psychiatry. 2021. PMID 34276447.
60. Menon V. Large-scale brain networks and psychopathology: a unifying triple network model. Trends Cogn Sci. 2011. PMID 21908230.
61. Chen P et al. Large-scale network abnormality in behavioral addiction. J Affect Disord. 2024. PMID 38521138.
62. Ma SS et al. Alterations in functional networks during cue-reactivity in internet gaming disorder. J Behav Addict. 2019. PMID 31146550.
63. Oldham S, Fornito A. The development of brain network hubs. Dev Cogn Neurosci. 2019. PMID 30579789.

64. Choe AS et al. Comparing test-retest reliability of dynamic functional connectivity methods. NeuroImage. 2017. PMID 28687517.
65. Ye B et al. Altered patterns of dynamic functional connectivity of brain networks in deficit and non-deficit schizophrenia. Eur Arch Psychiatry Clin Neurosci. 2025. PMID 38662092.
66. Murphy K, Fox MD. Towards a consensus regarding global signal regression for resting state functional connectivity MRI. NeuroImage. 2017. PMID 27888059.

Figures

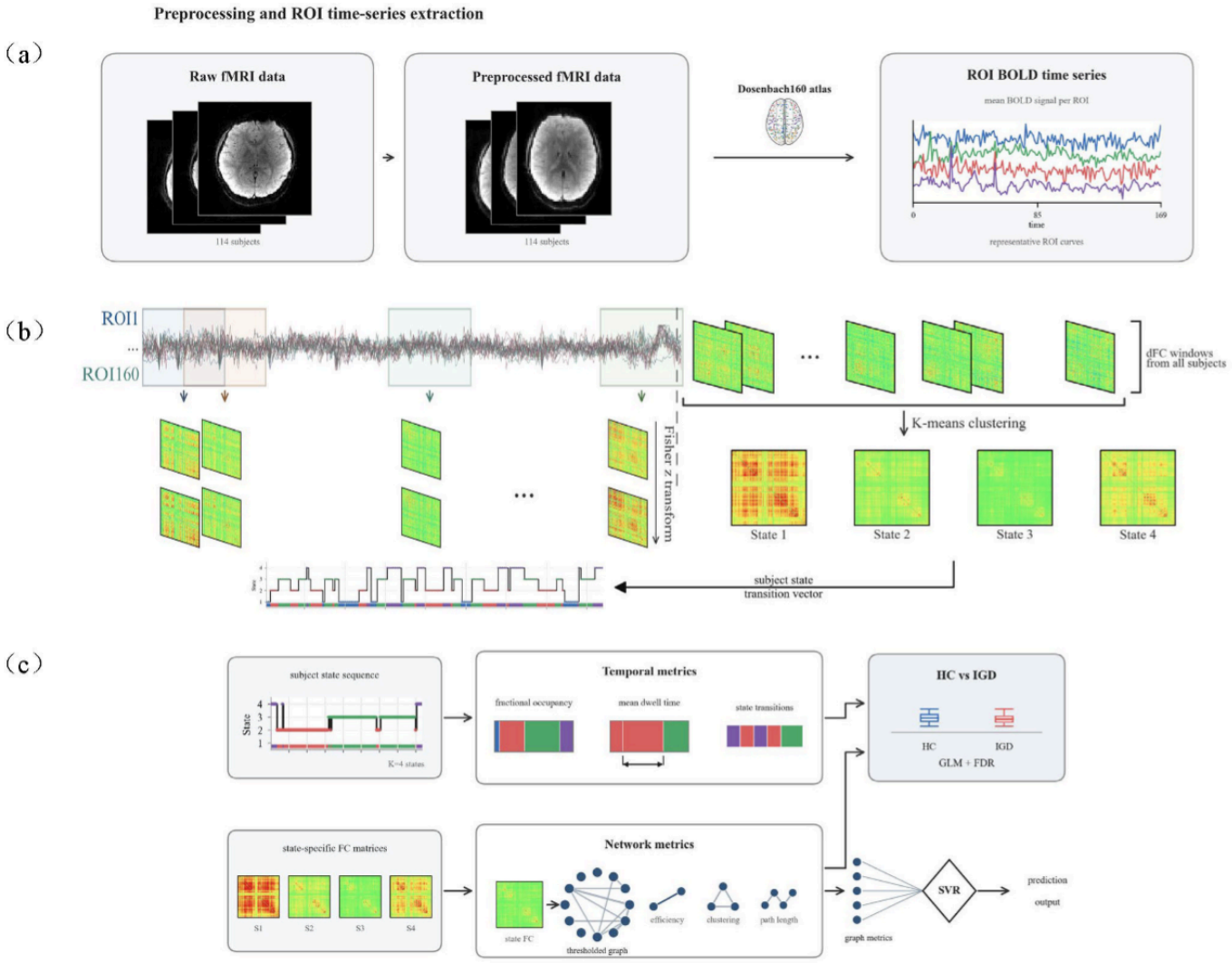
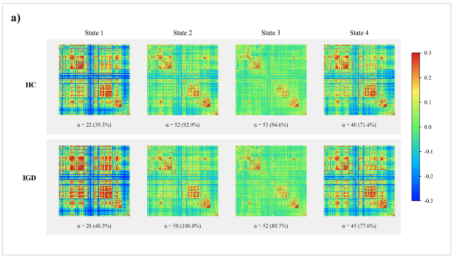
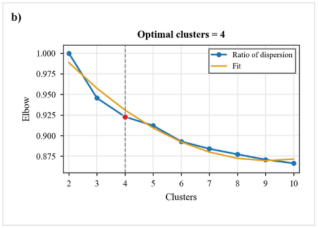


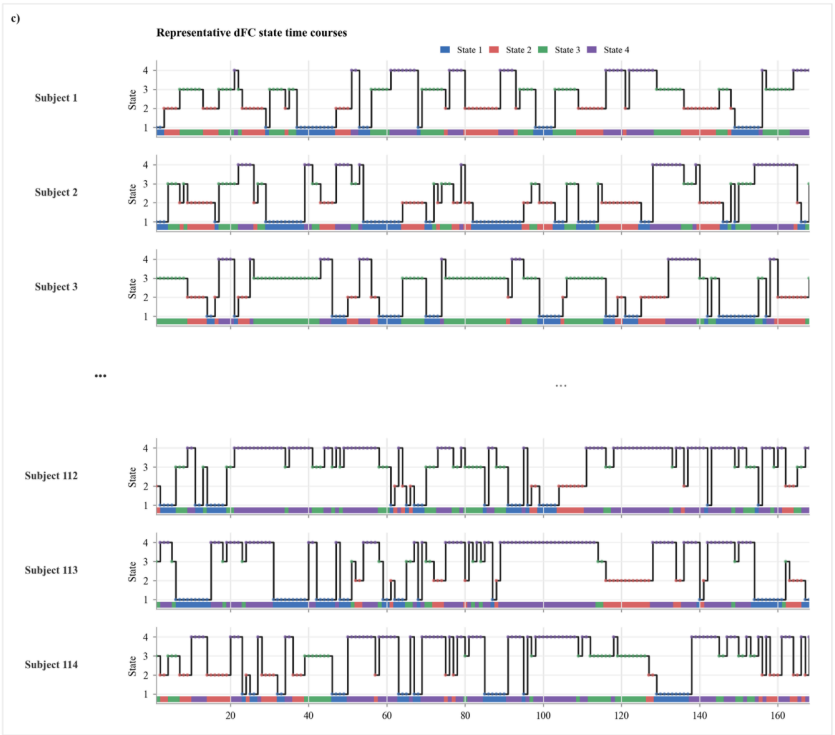
Figure 1

Dynamic functional-connectivity graph-theory analysis pipeline

Caption. (A; top) Raw fMRI data are preprocessed and parcellated into 160 Dosenbach ROI time series. (B; middle) Correlations from 60-TR sliding windows (2-TR step) are Fisher z-transformed and clustered into four states, producing a 168-window sequence per participant. (C; bottom) The sequences yield fractional occupancy, mean dwell time, and transitions; state-specific FC matrices yield graph metrics. These measures enter covariate-adjusted HC-IGD tests, and graph metrics additionally enter SVR prediction of IAT.







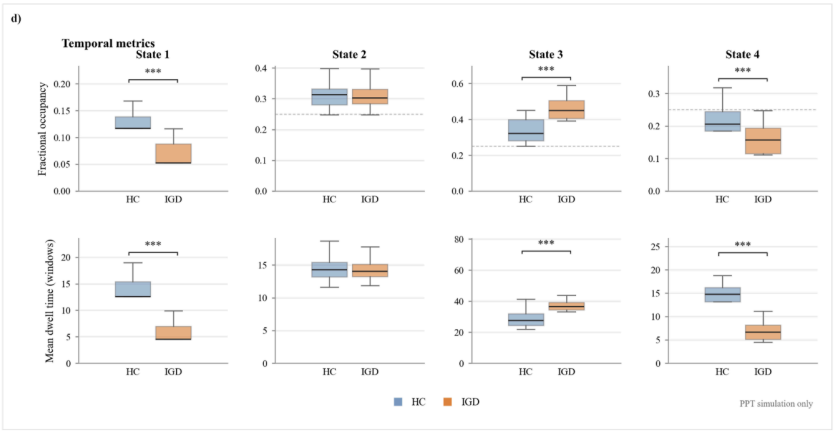


Figure 2

State-resolved dynamic connectivity overview and temporal illustration

Caption. (A) HC- and IGD-group mean Fisher z-transformed FC matrices for States 1-4; n (%) gives the number and proportion expressing each state. (B) The K-search elbow, with K = 4 selected. (C) Representative ordered 168-window state sequences; colours identify States 1-4. (D) Fractional occupancy (top) and mean dwell time (bottom): IGD values were lower in States 1 and 4, higher in State 3, and unchanged in State 2. Brackets denote group effects surviving 10,000 two-sided Freedman-Lane residual permutations with BH-FDR across nine temporal outcomes. Fractional occupancy includes all participants; mean dwell time includes state expressers only.

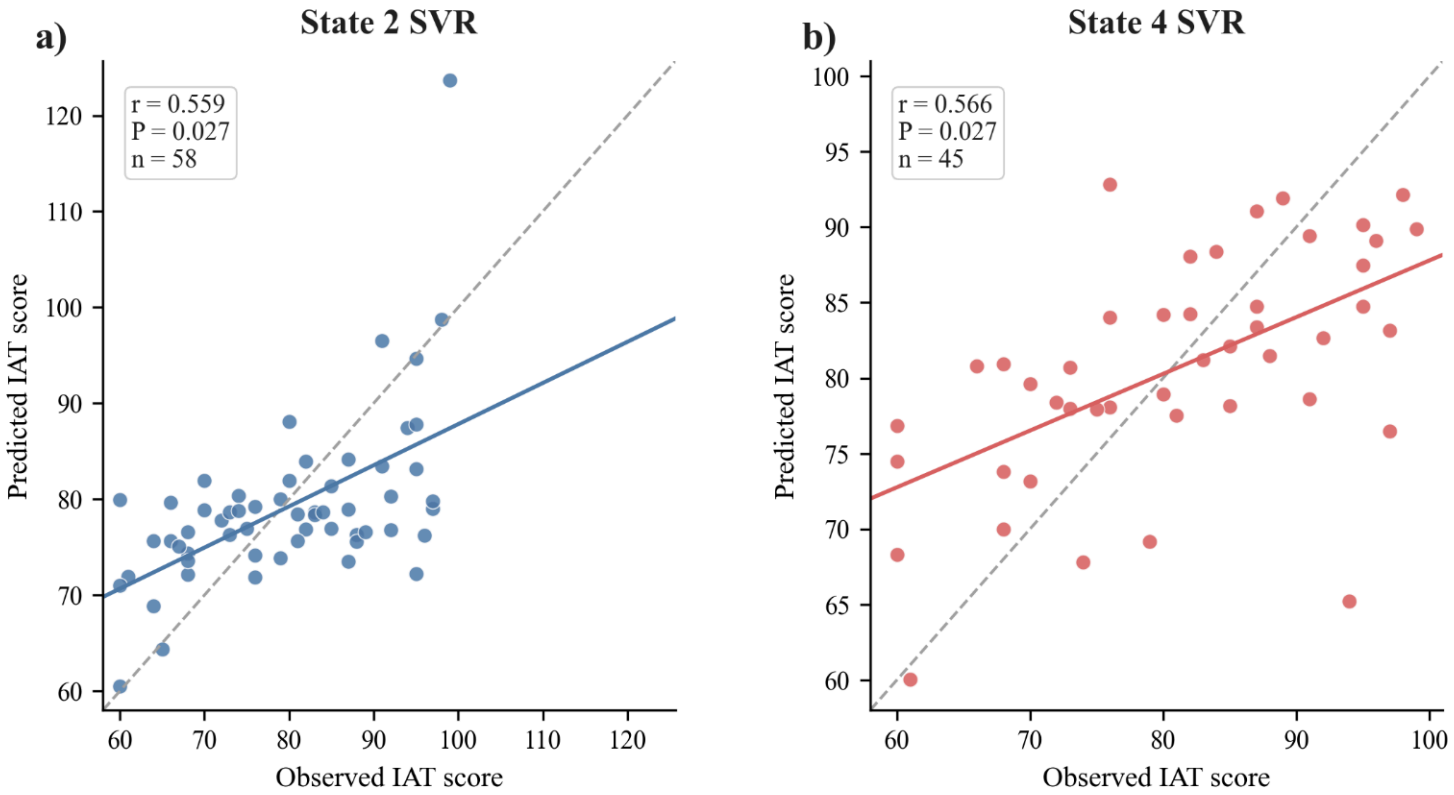


Figure 3

All-states IAT-SVR results for State 2 and State 4

Caption. Observed versus LOOCV-predicted IAT scores from state-specific linear SVR in IGD: (A) State 2 and (B) State 4. Points denote participants; solid and dashed lines denote the fitted and identity lines, respectively. Boxes report Pearson r, four-state FDR-adjusted permutation P, and n. IAT, Internet Addiction Test; LOOCV, leave-one-out cross-validation; SVR, support vector regression.

Supplementary Files

This is a list of supplementary files associated with this preprint. Click to download.

- Supplementary.docx